

Journal of Materials Chemistry A

Materials for energy and sustainability

Accepted Manuscript

This article can be cited before page numbers have been issued, to do this please use: X. Chen, Y. Kuwahara, K. Mori, C. Louis and H. Yamashita, *J. Mater. Chem. A*, 2020, DOI: 10.1039/C9TA11120D.



This is an Accepted Manuscript, which has been through the Royal Society of Chemistry peer review process and has been accepted for publication.

Accepted Manuscripts are published online shortly after acceptance, before technical editing, formatting and proof reading. Using this free service, authors can make their results available to the community, in citable form, before we publish the edited article. We will replace this Accepted Manuscript with the edited and formatted Advance Article as soon as it is available.

You can find more information about Accepted Manuscripts in the [Information for Authors](#).

Please note that technical editing may introduce minor changes to the text and/or graphics, which may alter content. The journal's standard [Terms & Conditions](#) and the [Ethical guidelines](#) still apply. In no event shall the Royal Society of Chemistry be held responsible for any errors or omissions in this Accepted Manuscript or any consequences arising from the use of any information it contains.

ARTICLE

Hydrophobic Titanium Doped Zirconium-based Metal Organic Framework for Photocatalytic Hydrogen Peroxide Production in Two-phase System

Received 00th January 20xx,
Accepted 00th January 20xx

DOI: 10.1039/x0xx00000x

Xiaolang Chen,^a Yasutaka Kuwahara,^{abc} Kohsuke Mori,^{ab} Catherine Louis,^d and Hiromi Yamashita^{*ab}

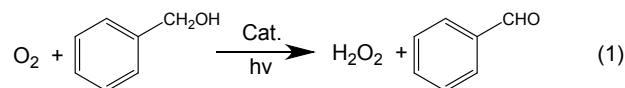
Photocatalytic synthesis of hydrogen peroxide (H₂O₂) from O₂ coupled with the synthesis of valuable products from benzyl alcohol (BA) by hydrophobic metal organic framework (MOF) is attractive. Herein, a hydrophobic titanium doped zirconium-based MOF (OPA/Zr_{100-x}Ti_x-MOF), whose metal Zr clusters were alkylated by octadecylphosphonic acid (OPA), was synthesized and used for photocatalytic H₂O₂ production in two-phase system (water/BA). This allows the formation of H₂O₂ in water phase and benzaldehyde, the oxidation product of BA, in the organic phase, respectively. The hydrophobic OPA/Zr_{92.5}Ti_{7.5}-MOF exhibited a remarkable H₂O₂ production rate of 9.7 mmol•L⁻¹•h⁻¹ under the irradiation of visible light (λ > 420 nm), which is about 4.5 times higher than that of the parent zirconium-based MOF (Zr₁₀₀-MOF). The enhanced activity is attributed to the effective Ti-doping and the unique hydrophobic nature of the catalyst. Ti species played the role of effectively promoting the electron transfer from photoexcited linkers of MOF to Ti, inhibiting the recombination of photogenerated electron-hole pairs in the hydrophobic MOF matrix. The unique hydrophobic nature, exemplified by a 139° of water contact angle, prevented overreduction of H₂O₂ by spatial separation of the MOF in BA and H₂O₂ in water. Recycling test of H₂O₂ production over the catalysts demonstrated that OPA/Zr_{92.5}Ti_{7.5}-MOF displayed a good stability. This study has greatly enriched the new application of hydrophobic MOFs in the field of photocatalytic energy production.

Introduction

Hydrogen peroxide (H₂O₂) can act as both multifunctional oxidant and reductant,¹ and is widely used in various chemical industries (like organic synthesis and paper-bleaching) and environmental treatment² (such as disinfection and water treatment).^{3, 4} Furthermore, H₂O₂ is a promising green and environmentally friendly energy alternative to hydrogen energy (H₂),⁵⁻⁷ and can be used in fuel cells.¹ H₂O₂ is more convenient and safer to be stored and transported than H₂ because of its higher water solubility.^{8, 9} As a potential energy carrier, the theoretical potential of aqueous H₂O₂ is 1.09 V, which is similar with that of a traditional H₂/O₂ fuel cell (1.23V).¹ The conventional anthraquinone method for H₂O₂ production meets some disadvantages such as high costs, complicated industrial routes, and substantial toxic by-products.¹⁰ Moreover, both electrocatalytic oxygen reduction reaction (ORR) route and the direct synthesis of H₂O₂ from H₂ and O₂ have

disadvantages such as high energy consumption or potentially explosive danger.¹¹⁻¹³ Therefore, it is necessary to explore a safer, more efficient, environmental-friendly and low-cost technology for H₂O₂ production.

Photocatalytic H₂O₂ production has recently attracted much attention due to its safety, eco-friendly consumption of low energy and pollution-free.^{1, 10, 14} Much efforts have been devoted to the photocatalytic H₂O₂ production by the reduction of O₂. For example, TiO₂,^{15, 16} CdS¹⁷ and g-C₃N₄-based^{1, 10} photocatalysts were reported to produce H₂O₂. However, the photocatalytic activity was still low, all of these systems produced only micromolar levels of H₂O₂ because of the wide bandgaps or low catalytic efficiency of photocatalysts.^{16, 18}



Metal organic frameworks (MOFs), consisting of organic linkers connected with metal oxide clusters, have been widely utilized in photocatalytic H₂ evolution,¹⁹ CO₂ reduction,²⁰ dye degradation²¹ as well as organic transformations²² due to their advantages, such as large surface area, tunable bandgap and well-defined crystalline structure, etc.²³⁻²⁵ Moreover, many MOFs have the property of absorbing visible light through their amine-functionalized linkers,²⁶ effectively improving the utilization rate of visible light. However, there are still few reports on the photocatalytic H₂O₂ production by MOFs. Recently, our group reported that photocatalytic H₂O₂ production coupled with oxidation of benzyl alcohol to benzaldehyde in two-phase system (equation (1)) was achieved successfully via the

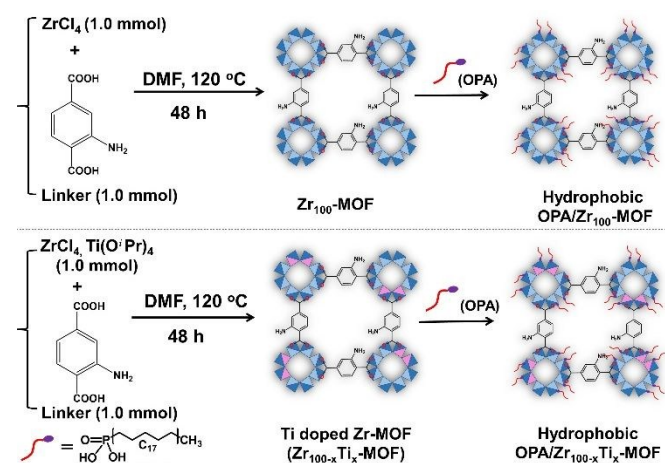
^a Graduate School of Engineering, Osaka University, 2-1 Yamadaoka, Suita, Osaka 565-0871, Japan. E-mail: yamashita@mat.eng.osaka-u.ac.jp

^b Elements Strategy Initiative for Catalysts and Batteries (ESICB), Kyoto University, Katsura, Kyoto 615-8520, Japan

^c JST, PRESTO, 4-1-8 Honcho, Kawaguchi, Saitama 332-0012, Japan

^d Sorbonne Universités, UPMC Univ Paris 06, UMR CNRS 7197, Laboratoire de Réactivité de Surface, 4 Place Jussieu, Tour 43-33, 3^{ème} étage, Case 178, F-75252 Paris, France

[†] Electronic Supplementary Information (ESI) available: BET, FTIR, XPS, TG-DTA data of the catalysts, the digital picture of samples in two-phase system, activity of H₂O₂ production in single-phase system, benzaldehyde concentration and characterization data of the used catalyst. See DOI: 10.1039/x0xx00000x



Scheme 1 Synthesis of Zr_{100} -MOF, OPA/ Zr_{100} -MOF, $Zr_{100-x}Ti_x$ -MOF and OPA/ $Zr_{100-x}Ti_x$ -MOF.

hydrophobization of MOFs.^{27, 28}

Zirconium-based MOF, due to its excellent structural stability, mechanical pressure and chemical properties, has attracted much attention in catalysis field.²⁹⁻³² In addition, partial substitution of Zr ions by doping with suitable metal ions as an electron mediator into MOFs can promote charge separation and prevent the recombination of photogenerated carriers in the MOF matrix.³³ For instance, Ti ions can effectively acts as active sites through a redox process of Ti^{4+} into Ti^{3+} in the photocatalytic reaction.^{34, 35} Based on this, we assumed that the combination of hydrophobic property of MOF with partially substituted Zr ions by Ti ions in a zirconium-based MOF (NH_2 -UiO-66(Zr)), which is relatively easy to be synthesized, will generate new catalysts for photocatalytic H_2O_2 production. Thus, Ti doped zirconium-based MOFs ($Zr_{100-x}Ti_x$ -MOF) were first synthesized with various of x . Then, octadecylphosphonic acid (OPA) with a long alkyl chain was used to coordinate metal Zr ions of clusters³⁶ (Scheme 1). Ultimately, hydrophobic Ti doped zirconium-based MOF (OPA/ $Zr_{100-x}Ti_x$ -MOF) was prepared. One of the samples, OPA/ $Zr_{92.5}Ti_{7.5}$ -MOF showed a 139° of water contact angle (exceeding 90°). Moreover, this hydrophobic catalyst was used into the two-phase system and brought about a remarkable H_2O_2 production rate of $9.7 \text{ mmol}\cdot\text{L}^{-1}\cdot\text{h}^{-1}$, which was about 4.5 times higher than that of the parent MOF (Zr_{100} -MOF).

Experiment section

Chemicals

2-Aminoterephthalic acid (98%), Oxo[5,10,15,20-tetra(4-pyridyl)porphinato]titanium(IV) ($[TiO(tpypH_4)]^{4+}$) (> 90%), and octadecylphosphonic acid (OPA) were supplied by Tokyo Chemical Industry Co., Ltd. (TCI). Hydrogen peroxide (30%), hydrochloric acid ($5 \text{ mol}\cdot\text{L}^{-1}$), perchloric acid (60%), acetonitrile (99%), zirconium tetrachloride ($ZrCl_4$, > 97%), N, N-dimethylformaldehyde (DMF, > 99.5%), ethanol (99.5%), methanol (> 99%) and benzyl alcohol (> 97%) were purchased from Nacalai Tesque. All chemicals were obtained commercially and utilized without further purification.

Catalysts preparation

Synthesis of Zr_{100} -MOF:

In a typical synthesis of NH_2 -UiO-66(Zr), $ZrCl_4$ (233.2 mg, 1.0 mmol) and 2-aminoterephthalic acid (181.2 g, 1.0 mmol) were dissolved in DMF (50 mL), subsequently, the solution was transferred to a 100 mL Teflon-lined stainless steel autoclave. The autoclave was sealed and heated in an oven at 120°C for 48 h, after cooling naturally of the oven in one hour, the samples were washed three time with DMF and centrifuged, then washed three times with anhydrous methanol and centrifuged, followed by dried under vacuum overnight at room temperature, and activated in vacuum at 120°C overnight to remove the solvent molecular in the MOFs. The pristine NH_2 -UiO-66(Zr) is denoted as Zr_{100} -MOF.

Synthesis of $Zr_{100-x}Ti_x$ -MOF:

The Ti doped NH_2 -UiO-66(Zr) were prepared according to the same procedure as above but with addition of varying amounts of Ti^{4+} (titanium isopropoxide was used as the Ti^{4+} precursor). The total amount of metals (Ti and Zr) was 1.0 mmol, and the selected molar ratios of $Ti/(Ti+Zr)$ were 5%, 7.5% and 10%. After synthesis, the samples were dealt with the same way as for Zr_{100} -MOF. The samples are denoted as $Zr_{95}Ti_5$ -MOF, $Zr_{92.5}Ti_{7.5}$ -MOF and $Zr_{90}Ti_{10}$ -MOF, respectively.

Synthesis of OPA/ $Zr_{100-x}Ti_x$ -MOF:

Unactivated MOFs (50 mg) were immersed in OPA ethanol solution (50 mL, 50 mM) for 24 h at room temperature. The suspension was stirred for 5 min every 2 h during the first 12 h. Then, it was centrifuged and washed several times with ethanol to remove free OPA. The washed samples were dried under vacuum at room temperature and activated in vacuum at 120°C overnight. The corresponding samples are denoted as OPA/ Zr_{100} -MOF, OPA/ $Zr_{95}Ti_5$ -MOF, OPA/ $Zr_{92.5}Ti_{7.5}$ -MOF and OPA/ $Zr_{90}Ti_{10}$ -MOF, respectively.

Material Characterization

Powder X-ray diffraction (XRD) was collected with a Rigaku Ultima IV diffractometer with $Cu\ K\alpha$ radiation ($\lambda = 1.54056 \text{ \AA}$). Ultraviolet visible diffuse reflectance spectra (UV-Vis DRS) was recorded by a Shimadzu UV-2450 spectrophotometer. $BaSO_4$ was used as the reference, and absorption spectra were obtained using the Kubelka-Munk function. Nitrogen adsorption measurements were performed using BELSORP-max system (Microtrac BEL Corp., Inc.) at -196°C . Samples were degassed under vacuum at 120°C for at least 6 h before data collection. TG-DTA was performed under air flow using a Rigaku thermogravimetry unit, Rigaku Thermo Plus EVO II series high-temperature differential thermal balance TG/DTA, with temperature ramp of $1.0^\circ\text{C}\ \text{min}^{-1}$ up to 800°C . Fourier transform infrared spectroscopy (FT-IR) was carried out with a JASCO FTIR-6100 by measuring the plates of MOFs added into KBr. X-ray photoelectron spectra (XPS) was performed with a Shimadzu XPS system, ESCA-3400, using the Mg K line (1253.6 eV). Binding energy was calibrated using C 1s photoelectronic peak at 285 eV . Photoluminescence measurements were performed using a fluorolog-3 spectrofluorometer (Horiba).

Photocatalytic reaction

In a typical photocatalytic reaction setup for two-phase system: the photocatalysts (5.0 mg), water (2.0 mL) and benzyl alcohol (BA) (5.0 mL) were added to a Pyrex[®] reaction vessel (30 mL), which was sealed with a rubber septum. The resulting mixture was sonicated for about 5 min to disperse the photocatalyst, then bubbled with oxygen for 15 min with a rate of 20 mL•min⁻¹ under magnetic stirring in the dark. Subsequently, the reaction vessel was irradiated from the side with a Xe lamp (500 W; SANEI ELECTRIC XEF-501S) through a glass filter ($\lambda > 420$ nm) under magnetic stirring at ambient pressure and temperature. The distance between the light source and reaction vessel was approximately 2 cm. An aliquot of solution was collected from the reaction mixture every one hour and analysed.

In a photocatalytic reaction setup for single-phase system: the photocatalysts (5.0 mg), acetonitrile (5.0 mL) and BA (1.0 mL) were added to a Pyrex[®] reaction vessel (30 mL), then the next procedures were same as above two-phase system.

Recycling test

The MOFs (10 mg) were added to the two-phase system composed of water (4.0 mL) and benzyl alcohol (10 mL). The mixture was bubbled with oxygen for 15 min with a rate of 20 mL•min⁻¹ in the dark. Then, the system was irradiated with visible light ($\lambda > 420$ nm). After 3 h, the quantification of H₂O₂ was detected and the reaction suspension was transferred to the centrifuge tube from reaction vessel, washed three times with ethanol and centrifuged to collect the MOFs. The collected MOFs were dried in vacuum at room temperature overnight. After that, benzyl alcohol (10 mL) was added into the centrifuge tube, then the mixture was sonicated to get the suspension, which was transferred to the reaction vessel for next cycle.

Quantification of produced H₂O₂

The amount of produced H₂O₂ was determined by spectroscopic titration with an acidic solution of [TiO(tpypH₄)]⁴⁺ complex (Ti-TPYP reagent) according to the literature.³⁷ The Ti-TPYP reagent (34 mg) was dissolved in 1.0 L of 50 mM hydrochloric acid. An aliquot (e.g., 10 μ L) from original reaction solution was diluted in a given volume of distilled water and utilized as a sample solution. 0.25 mL of Ti-TPYP reagent and 0.25 mL of 4.8 M perchloric acid were added into 0.25 mL of the sample solution. After waiting 5 min at room temperature, the mixture was diluted to 2.5 mL with distilled water and used for the spectroscopic measurement. Absorbance at $\lambda = 434$ nm was measured using the Shimadzu UV-2600 UV-Vis spectrophotometer (A_S). A similar way, a blank solution, whose absorbance designated as A_B, was prepared by using distilled water instead of the sample solution. The difference in absorbance was calculated by following the equation: $\Delta A_{434} = A_B - A_S$. Based on ΔA_{434} and the volume of solution, the amount of H₂O₂ was deduced.

The amount of produced benzaldehyde was analysed by gas chromatography (Shimadzu, GC-14B with Phenomenex ZB-FFAP columns).

Results and discussion

X-ray diffraction (XRD) patterns of the synthesized samples were shown in Fig. 1a and b. They only display the characteristic diffraction peaks of pristine Zr₁₀₀-MOF but with weakened peak intensities due to Ti-doping and addition of OPA. No other peaks associated with Ti⁴⁺ oxides or Ti-related impurities can be observed. This preliminary indicates that the MOFs was doped by Ti ions.

In addition, the UV-Vis DRS were shown in Fig. 1c and d. Both Zr_{100-x}Ti_x-MOF and OPA/Zr_{100-x}Ti_x-MOF generally inherited the optical absorption characteristics of the parent Zr₁₀₀-MOF. The absorption bands in the high energy region ($\lambda < 300$ nm) can be assigned to the $\pi \rightarrow \pi^*$ transition of the linker, while the absorption band extending to the visible region from 320 to 450 nm is originated from the ligand-to-cluster charge transfer (LCCT) of amino functional group (-NH₂) on the organic linkers.^{38, 39} It indicates that all of the samples have the visible-light-responsive characteristic, which is suitable for the photocatalytic reaction induced by visible light. After doping with Ti ions, the absorption edge position of MOFs slightly shifted to lower wavelength compared with the sample without Ti doping because of the generation of several energy bands between the lowest unoccupied molecular orbital (LUMO) and highest occupied molecular orbital (HOMO) states, confirming the successful substitution of Ti ions.²⁶

The N₂ adsorption/desorption isotherms and Brunauer-Emmett-Teller (BET) surface areas were shown in Fig. S1 and Table S1. All samples exhibited a type I sorption isotherm, indicating a typical microporous structure. The BET surface areas of Zr_{100-x}Ti_x-MOF continue to decrease as the amount of Ti-doping increases, respectively, compared with that of Zr₁₀₀-MOF. OPA/Zr_{100-x}Ti_x-MOF has the similar trend, compared with that of OPA/Zr₁₀₀-MOF. This could be resulted from the loss of the well-ordered structure due to Ti-doping, as confirmed by the XRD (Fig. 1a and b). Additionally, the BET surface areas of Zr_{100-x}Ti_x-MOF also decreases after modification

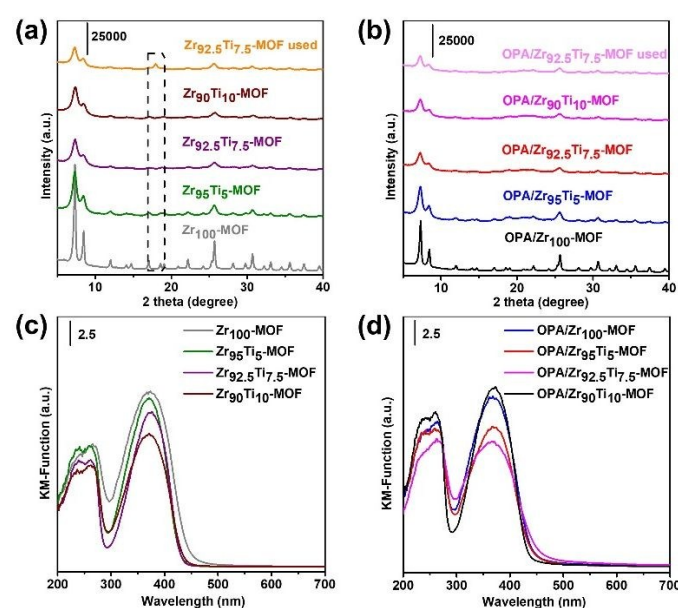


Fig. 1 XRD patterns of (a) Zr_{100-x}Ti_x-MOF and (b) OPA/Zr_{100-x}Ti_x-MOF before and after used. UV-vis DRS of (c) Zr_{100-x}Ti_x-MOF and (d) OPA/Zr_{100-x}Ti_x-MOF.

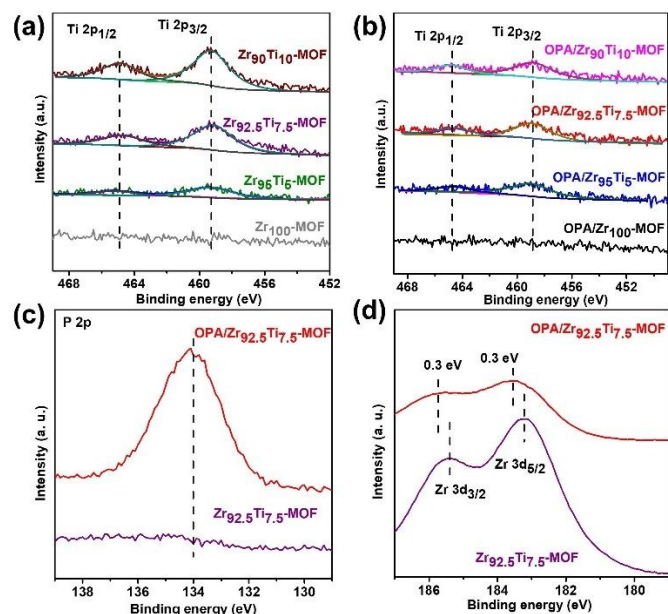


Fig. 2 XPS spectra of the synthesized samples: Ti 2p of (a) $Zr_{100-x}Ti_x$ -MOF and (b) OPA/ $Zr_{100-x}Ti_x$ -MOF. (c) P 2p of $Zr_{92.5}Ti_{7.5}$ -MOF and OPA/ $Zr_{92.5}Ti_{7.5}$ -MOF. (d) Zr 3d of $Zr_{92.5}Ti_{7.5}$ -MOF and OPA/ $Zr_{92.5}Ti_{7.5}$ -MOF.

by OPA, compared with that of OPA/ $Zr_{100-x}Ti_x$ -MOF. This is due to the modification of OPA into the interior of MOFs, as verified by the reduced pore volume.

The chemical states of Ti, P and Zr elements in $Zr_{100-x}Ti_x$ -MOF and OPA/ $Zr_{100-x}Ti_x$ -MOF were determined by XPS in Fig. 2a, the peaks at around 459.0 eV and 465.0 eV attributed to the Ti 2p_{3/2} and Ti 2p_{1/2}, respectively, further confirm the Ti⁴⁺-doping in $Zr_{100-x}Ti_x$ -MOF and OPA/ $Zr_{100-x}Ti_x$ -MOF. As the amount of Ti increases, the corresponding peak signals are stronger. Furthermore, the corresponding peak intensities of Ti⁴⁺ are more weakened in the hydrophobic OPA/ $Zr_{100-x}Ti_x$ -MOF in Fig. 2b. This could be due to the modification of OPA into both surface and interior of MOFs, resulted in weaker signals. Additionally, the XPS peaks of P 2p at around 134.0 eV for Zr_{100} -MOF, OPA/ Zr_{100} -MOF, $Zr_{92.5}Ti_{7.5}$ -MOF and OPA/ $Zr_{92.5}Ti_{7.5}$ -MOF were also shown in Fig. S2 and Fig. 2c. It further indicates that the MOFs are modified by OPA successfully, which is consistent with the results of FT-IR spectra in Fig. S3. Two peaks assigned to the symmetric and asymmetric stretching vibration of CH₂ in the alkyl -CH₂- groups of OPA are observed at around 2920 and 2850 cm⁻¹ in the FT-IR spectra of OPA/ $Zr_{100-x}Ti_x$ -MOF (Fig. S3b), which are not observed in the spectra of $Zr_{100-x}Ti_x$ -MOF (Fig. S3a). Moreover, the binding energies of Zr 3d in OPA/ $Zr_{92.5}Ti_{7.5}$ -MOF both show positive shifts of 0.3 eV, compared to that of $Zr_{92.5}Ti_{7.5}$ -MOF in Fig. 2d. The same result for OPA/ Zr_{100} -MOF and Zr_{100} -MOF was shown in Fig. S4. This result demonstrates an interaction between OPA and the Zr atoms of metal clusters, resulting from the formation of Zr-O-P³⁶ in OPA/ $Zr_{92.5}Ti_{7.5}$ -MOF and OPA/ Zr_{100} -MOF, sustaining the alkylation of Zr clusters by OPA. TG-DTA measurements in Fig. S5 revealed that 7.3 % and 8.7 % of the Zr atoms in the clusters were alkylated by OPA for OPA/ Zr_{100} -MOF and OPA/ $Zr_{92.5}Ti_{7.5}$ -MOF, respectively.

The hydrophobicity of MOFs was examined by measuring their water contact angles (Fig. 3). The water contact angles of Zr_{100} -MOF and $Zr_{92.5}Ti_{7.5}$ -MOF are 30° and 0° (Fig. 3a and c), respectively,

indicating their hydrophilic property. By contrast, the water contact angles for OPA/ Zr_{100} -MOF and OPA/ $Zr_{92.5}Ti_{7.5}$ -MOF are 127° and 139° (Fig. 3b and d). The higher water contact angles exceeding 90° indicate that OPA has transformed MOFs into hydrophobic materials.

The photoluminescence (PL) measurements were further performed to verify the intrinsic role of Ti dopant in MOFs during the photocatalysis. The corresponding PL emission spectra of Ti doped MOFs are shown in Fig. 4a and b. $Zr_{92.5}Ti_{7.5}$ -MOF and OPA/ $Zr_{92.5}Ti_{7.5}$ -MOF both show weaker PL emission intensities than Zr_{100} -MOF and OPA/ Zr_{100} -MOF without Ti dopant. This result confirms that Ti dopant effectively promotes electrons transfer, inhibiting the recombination of electron-hole pairs in the photoexcited MOFs.⁴⁰⁻⁴²

H₂O₂ production in two-phase system was performed under visible light irradiation ($\lambda > 420$ nm). The hydrophilic $Zr_{100-x}Ti_x$ -MOF was dispersed in aqueous phase, while hydrophobic OPA/ $Zr_{100-x}Ti_x$ -MOF was dispersed in BA phase (Fig. S6). When H₂O₂ was produced, it was concentrated in aqueous phase, while benzaldehyde, the oxidation product of BA in the BA phase. The concentration of H₂O₂ on a certain time are shown in Fig. 4c and d. Hydrophobic OPA/ $Zr_{100-x}Ti_x$ -MOF showed higher activity of H₂O₂ production (Fig. 4d) than hydrophilic $Zr_{100-x}Ti_x$ -MOF (Fig. 4c), reflecting the better catalytic performance of hydrophobic MOFs. Usually, overreduction of H₂O₂ to OH⁻ and •OH occur during photocatalysis, which results in lowering H₂O₂ production. Spatial separation of MOFs and produced H₂O₂ suppresses this phenomenon.²⁸ To illustrate this point, H₂O₂ decomposition in two-phase system was measured and the results are shown in Fig. 5a. OPA/ $Zr_{92.5}Ti_{7.5}$ -MOF showed higher H₂O₂ concentration than $Zr_{92.5}Ti_{7.5}$ -MOF, demonstrating that the hydrophobic MOF in organic phase does inhibit the overreduction of H₂O₂. Additionally, OPA/ $Zr_{92.5}Ti_{7.5}$ -MOF have better activity than other OPA modified MOFs (Fig. 4d). Similar trend was shown in Fig. 4c for $Zr_{92.5}Ti_{7.5}$ -MOF. It illustrates that doping Ti with a molar rate of 7.5% is optimal. Hence, Ti species plays a crucial role in the improvement of activity for H₂O₂ production. Finally, the hydrophobic OPA/ $Zr_{92.5}Ti_{7.5}$ -MOF possesses a H₂O₂ production rate of 9.7 mmol•L⁻¹•h⁻¹, which is about 4.5 times higher than that of the pristine Zr_{100} -MOF. A further increase of doping amount of Ti leads to a significant decrease of activity, which can be attributed to the lower crystallinities, as confirmed by XRD (Fig. 1a and b) and decreased surface areas (Table S1) of samples. Specially, the formed •O₂⁻ inside MOFs will not be diffused well to the aqueous phase to form H₂O₂ due to the smaller surface areas and smaller pore volume.

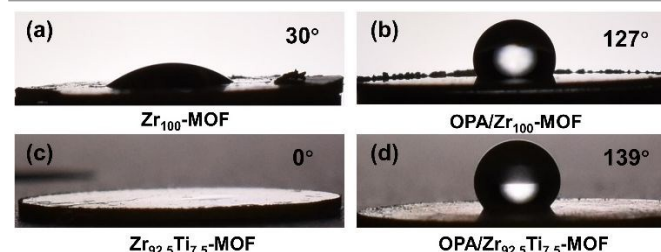


Fig. 3 The water contact angles of Zr_{100} -MOF, OPA/ Zr_{100} -MOF, $Zr_{92.5}Ti_{7.5}$ -MOF and OPA/ $Zr_{92.5}Ti_{7.5}$ -MOF (20 μ L of water droplets on tablets of MOFs, the tablets were produced by pressing corresponding \sim 20 mg of MOFs at 10 MPa for 5 min).

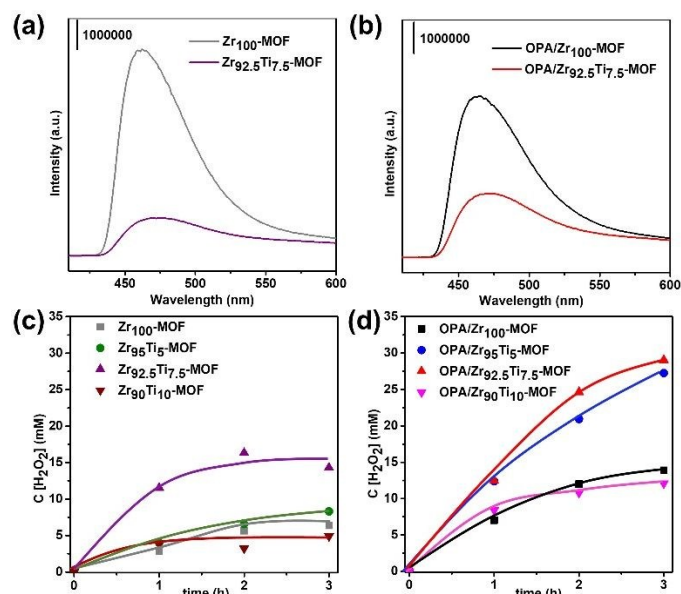


Fig. 4 The Photoluminescence (PL) emission spectra ($\lambda_{\text{ex}} = 400 \text{ nm}$) of (a) $\text{Zr}_{100}\text{-MOF}$ and $\text{Zr}_{92.5}\text{Ti}_{7.5}\text{-MOF}$, (b) $\text{OPA/Zr}_{100}\text{-MOF}$ and $\text{OPA/Zr}_{92.5}\text{Ti}_{7.5}\text{-MOF}$. Time courses of H_2O_2 production of (c) hydrophilic $\text{Zr}_{100-x}\text{Ti}_x\text{-MOF}$ and (d) hydrophobic $\text{OPA/Zr}_{100-x}\text{Ti}_x\text{-MOF}$ under photoirradiation ($\lambda > 420 \text{ nm}$) of two-phase system composed of BA (5.0 mL) and water (2.0 mL) catalyzed by 5.0 mg of photocatalysts.

This can be further verified in Fig. S7. H_2O_2 production utilizing $\text{Zr}_{100}\text{-MOF}$ and $\text{OPA/Zr}_{100}\text{-MOF}$ was examined in a single-phase system, which was composed of an acetonitrile solution (5.0 mL) of BA (1.0 mL). $\text{OPA/Zr}_{100}\text{-MOF}$ displayed lower activity than $\text{Zr}_{100}\text{-MOF}$ due to the much lower surface areas and smaller pore volume caused by modification of OPA. Similarly, this may also influence the diffusion of produced benzaldehyde, resulting in lower detectable concentration of benzaldehyde (Fig. S8) than that of H_2O_2 production after 3 h of reaction.

Results of recycling tests were displayed in Fig. 5b. $\text{OPA/Zr}_{92.5}\text{Ti}_{7.5}\text{-MOF}$ still remains high activity of H_2O_2 production after 7 cycles of experiment, while $\text{Zr}_{92.5}\text{Ti}_{7.5}\text{-MOF}$ shows a continuous decrease. This is due to the more stable structure of hydrophobic MOF in organic phase, while the structure of hydrophilic MOF in the aqueous phase could be destroyed, as verified by XRD of the samples before and after recycling tests (Fig. 1 and S9a). It reveals that the characteristic diffraction peaks of $\text{OPA/Zr}_{92.5}\text{Ti}_{7.5}\text{-MOF}$ are maintained substantially, indicating its intact structure is remained, whereas the peak intensity for $\text{Zr}_{92.5}\text{Ti}_{7.5}\text{-MOF}$ is weakened, and an impurity peak at 18° has appeared. The FTIR of $\text{OPA/Zr}_{92.5}\text{Ti}_{7.5}\text{-MOF}$ before and after

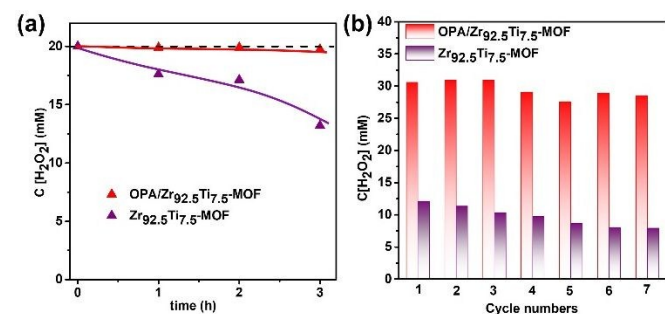


Fig. 5 (a) Time courses of H_2O_2 (20 mM) decomposition in two-phase system at room temperature in dark. (b) Recycling tests of $\text{Zr}_{92.5}\text{Ti}_{7.5}\text{-MOF}$ and $\text{OPA/Zr}_{92.5}\text{Ti}_{7.5}\text{-MOF}$.

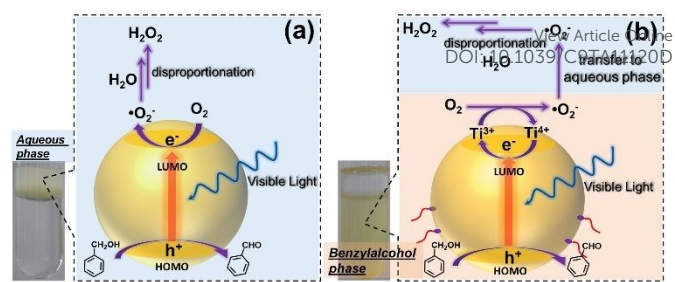


Fig. 6 The proposed mechanism for photocatalytic H_2O_2 production of (a) $\text{Zr}_{100}\text{-MOF}$ and (b) $\text{OPA/Zr}_{92.5}\text{Ti}_{7.5}\text{-MOF}$.

reaction indicates that two peaks at around 2920 and 2850 cm^{-1} of CH_2 in the alkyl $-\text{CH}_2-$ groups in OPA are retained (Fig. S9b), implying that its hydrophobic nature is maintained. These results adequately demonstrate that $\text{OPA/Zr}_{92.5}\text{Ti}_{7.5}\text{-MOF}$ is stable in the two-phase system.

Based on the above results, a reaction mechanism was proposed in Fig. 6. For hydrophilic $\text{Zr}_{100}\text{-MOF}$ without Ti-doping (Fig. 6a), photoexcited electrons formed and gathered in the LUMO after the absorption of visible light by the linker,^{43,44} while photoexcited holes generated in the HOMO.⁴⁴ Photoexcited electrons in LUMO would reduce O_2 to $\bullet\text{O}_2^-$, while photogenerated holes in HOMO were quenched by the oxidation of benzyl alcohol to benzaldehyde. The $\bullet\text{O}_2^-$ then formed H_2O_2 through disproportionation process^{28, 45} in aqueous phase. However, the recombination of photoexcited electrons and holes is prone to happen due to the lack of an effective LCCT mechanism.^{44, 46} In addition, the hydrophilic MOF would inevitably decompose H_2O_2 when both the catalyst and H_2O_2 are in the same phase. Those factors cause an undesirable activity decrease. In contrast, the LCCT mechanism is effectively constructed after Ti-doping in hydrophobic $\text{OPA/Zr}_{92.5}\text{Ti}_{7.5}\text{-MOF}$. The doped Ti^{4+} ions in clusters were reduced to Ti^{3+} by the photoexcited electrons in LUMO of hydrophobic $\text{OPA/Zr}_{92.5}\text{Ti}_{7.5}\text{-MOF}$ (Fig. 6b). Then, the reduction of O_2 to $\bullet\text{O}_2^-$ by Ti^{3+} was achieved, while photogenerated holes in HOMO were quenched by the oxidation of benzyl alcohol to benzaldehyde. We have already reported that in two-phase reaction system, $\bullet\text{O}_2^-$ would transfer to the aqueous phase before it formed H_2O_2 in aqueous phase.²⁸ It should be pointed out that the Ti^{4+} species in the MOF played a vital role in promoting the photogenerated charge transfer from MOF thanks to the redox reaction of $\text{Ti}^{4+}/\text{Ti}^{3+}$, inhibiting the recombination of photogenerated electron-hole pairs. Additionally, the spatial separation of the MOF and H_2O_2 prevented overreduction of H_2O_2 , also resulting in a higher activity.

Conclusions

Hydrophobic Ti doped $\text{NH}_2\text{-UiO-66(Zr)}$ was synthesized and used to produce H_2O_2 in a two-phase system. Doping with Ti species promotes the photogenerated electrons transfer and inhibits the recombination of the photogenerated electron-hole pairs in the MOFs, bringing about an improved activity of H_2O_2 production. The hydrophobic nature of MOFs allows the spatial separation of the photocatalyst while produced H_2O_2 is transferred to water phase.

This is beneficial for inhibiting the overreduction of H₂O₂, and results in an enhanced activity for H₂O₂ production. Furthermore, the hydrophobic MOF sustains a good stability in the recycling tests. This study greatly extended the application of hydrophobic MOFs in the field of photocatalytic H₂O₂ production.

Conflicts of interest

There are no conflicts to declare.

Acknowledgements

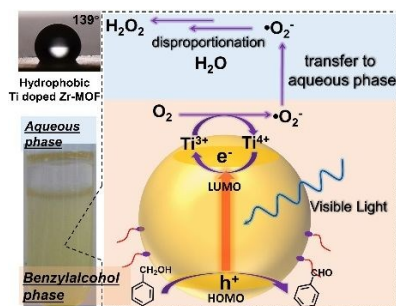
The present work was supported by the Grant-in-Aid for Scientific Research from the Ministry of Education, Culture, Sports, Science and Technology (MEXT) of Japan (26220911). Part of this work was performed under the management of "Elements Strategy Initiative for Catalysts and Batteries (ESICB)" supported by the MEXT, Japan.

Notes and references

- 1 Y. Kofuji, Y. Isobe, Y. Shiraishi, H. Sakamoto, S. Tanaka, S. Ichikawa and T. Hirai, *J. Am. Chem. Soc.*, 2016, **138**, 10019-10025.
- 2 J. M. Campos-Martin, G. Blanco-Brieva and J. L. G. Fierro, *Angew. Chem., Int. Ed.*, 2006, **45**, 6962-6984.
- 3 Z. W. Seh, J. Kibsgaard, C. F. Dickens, I. Chorkendorff, J. K. Nørskov and T. F. Jaramillo, *Science*, 2017, **355**, eaad4998.
- 4 S. Siahrostami, A. Verdaguier-Casadevall, M. Karamad, D. Deiana, P. Malacrida, B. Wickman, M. Escudero-Escribano, E. A. Paoli, R. Frydendal, T. W. Hansen, I. Chorkendorff, I. E. L. Stephens and J. Rossmeisl, *Nat. Mater.*, 2013, **12**, 1137.
- 5 Y. Zheng, Z. Yu, H. Ou, A. M. Asiri, Y. Chen and X. Wang, *Adv. Funct. Mater.*, 2018, **28**, 1705407.
- 6 S. Zhao, T. Guo, X. Li, T. Xu, B. Yang and X. Zhao, *Appl. Catal., B*, 2018, **224**, 725-732.
- 7 H. Yin, Y. Kuwahara, K. Mori and H. Yamashita, *J. Mater. Chem. A*, 2018, **6**, 10932-10938.
- 8 S. Zhao and X. Zhao, *J. Catal.*, 2018, **366**, 98-106.
- 9 S. Zhao and X. Zhao, *Appl. Catal., B*, 2019, **250**, 408-418.
- 10 Z. Wei, M. Liu, Z. Zhang, W. Yao, H. Tan and Y. Zhu, *Energy Environ. Sci.*, 2018, **11**, 2581-2589.
- 11 Z. Zheng, Y. H. Ng, D.-W. Wang and R. Amal, *Adv. Mater.*, 2016, **28**, 9949-9955.
- 12 J. C. Pritchard, Q. He, E. N. Ntainjua, M. Piccinini, J. K. Edwards, A. A. Herzing, A. F. Carley, J. A. Moulijn, C. J. Kiely and G. J. Hutchings, *Green Chem.*, 2010, **12**, 915-921.
- 13 N. M. Wilson and D. W. Flaherty, *J. Am. Chem. Soc.*, 2016, **138**, 574-586.
- 14 H. i. Kim, O. S. Kwon, S. Kim, W. Choi and J. H. Kim, *Energy Environ. Sci.*, 2016, **9**, 1063-1073.
- 15 G. h. Moon, W. Kim, A. D. Bokare, N. e. Sung and W. Choi, *Energy Environ. Sci.*, 2014, **7**, 4023-4028.
- 16 Y. Shiraishi, S. Kanazawa, D. Tsukamoto, A. Shiro, Y. Sugano and T. Hirai, *ACS Catal.*, 2013, **3**, 2222-2227.
- 17 S. Thakur, T. Kshetri, N. H. Kim and J. H. Lee, *J. Catal.*, 2017, **345**, 78-86.
- 18 R. Nakamura, A. Imanishi, K. Murakoshi and Y. Nakato, *J. Am. Chem. Soc.*, 2003, **125**, 7443-7450.
- 19 K. Meyer, M. Ranocchiari and J. A. van Bokhoven, *Energy Environ. Sci.*, 2015, **8**, 1923-1937.
- 20 Y. Chen, D. Wang, X. Deng and Z. Li, *Catal. Sci. Technol.*, 2017, **7**, 4893-4904.
- 21 C.-C. Wang, J.-R. Li, X.-L. Lv, Y.-Q. Zhang and G. Guo, *Energy Environ. Sci.*, 2014, **7**, 2831-2867. DOI: 10.1039/C9TA11120D
- 22 X. Deng, Z. Li and H. García, *Chem. Eur. J.*, 2017, **23**, 11189-11209.
- 23 Z. L. Wu, C. H. Wang, B. Zhao, J. Dong, F. Lu, W. H. Wang, W. C. Wang, G. J. Wu, J. Z. Cui and P. Cheng, *Angew. Chem., Int. Ed.*, 2016, **55**, 4938-4942.
- 24 T. Zhang and W. Lin, *Chem. Soc. Rev.*, 2014, **43**, 5982-5993.
- 25 W. Wang, X. Xu, W. Zhou and Z. Shao, *Adv. Sci.*, 2017, **4**, 1600371.
- 26 M. Wen, K. Mori, Y. Kuwahara and H. Yamashita, *ACS Energy Lett.*, 2017, **2**, 1-7.
- 27 Y. Kawase, Y. Isaka, Y. Kuwahara, K. Mori and H. Yamashita, *Chem. Commun.*, 2019, **55**, 6743-6746.
- 28 Y. Isaka, Y. Kawase, Y. Kuwahara, K. Mori and H. Yamashita, *Angew. Chem., Int. Ed.*, 2019, **58**, 5402-5406.
- 29 Y. Han, M. Liu, K. Li, Q. Sun, W. Zhang, C. Song, G. Zhang, Z. Conrad Zhang and X. Guo, *Inorg. Chem. Front.*, 2017, **4**, 1870-1880.
- 30 J. H. Cavka, S. Jakobsen, U. Olsbye, N. Guillou, C. Lamberti, S. Bordiga and K. P. Lillerud, *J. Am. Chem. Soc.*, 2008, **130**, 13850-13851.
- 31 L. Valenzano, B. Civalieri, S. Chavan, S. Bordiga, M. H. Nilsen, S. Jakobsen, K. P. Lillerud and C. Lamberti, *Chem. Mater.*, 2011, **23**, 1700-1718.
- 32 Y. Kuwahara, H. Kango and H. Yamashita, *ACS Sustain. Chem. Eng.* 2017, **5**, 1141-1152.
- 33 M. A. Syzgantseva, C. P. Ireland, F. M. Ebrahim, B. Smit and O. A. Syzgantseva, *J. Am. Chem. Soc.*, 2019, **141**, 6271-6278.
- 34 D. Sun, W. Liu, M. Qiu, Y. Zhang and Z. Li, *Chem. Commun.*, 2015, **51**, 2056-2059.
- 35 A. Santiago Portillo, H. G. Baldoví, M. T. García Fernandez, S. Navalón, P. Atienzar, B. Ferrer, M. Alvaro, H. Garcia and Z. Li, *J. Phys. Chem. C* 2017, **121**, 7015-7024.
- 36 Y. Sun, Q. Sun, H. Huang, B. Aguila, Z. Niu, J. A. Perman and S. Ma, *J. Mater. Chem. A*, 2017, **5**, 18770-18776.
- 37 C. Matsubara, N. Kawamoto and K. Takamura, *Analyst*, 1992, **117**, 1781-1784.
- 38 D. Sun, Y. Fu, W. Liu, L. Ye, D. Wang, L. Yang, X. Fu and Z. Li, *Chem.-Eur. J.*, 2013, **19**, 14279-14285.
- 39 C. Silva, I. Luz, X. Llabres, A. Corma and H. Garcia, *Chem.*, 2010, **16**, 11133-11138.
- 40 J. D. Xiao, Q. Shang, Y. Xiong, Q. Zhang, Y. Luo, S. H. Yu and H. L. Jiang, *Angew. Chem., Int. Ed.*, 2016, **55**, 9389-9393.
- 41 M. D. L. Ruiz Peralta, U. Pal and R. S. Zeferino, *ACS Appl. Mater. Inter.*, 2012, **4**, 4807-4816.
- 42 J. D. Xiao, L. Han, J. Luo, S. H. Yu and H. L. Jiang, *Angew. Chem., Int. Ed.*, 2018, **57**, 1103-1107.
- 43 M. Wen, Y. Kuwahara, K. Mori, D. Zhang, H. Li and H. Yamashita, *J. Mater. Chem. A*, 2015, **3**, 14134-14141.
- 44 S. Yuan, J. S. Qin, H. Q. Xu, J. Su, D. Rossi, Y. Chen, L. Zhang, C. Lollar, Q. Wang, H. L. Jiang, D. H. Son, H. Xu, Z. Huang, X. Zou and H. C. Zhou, *ACS Central Sci.*, 2018, **4**, 105-111.
- 45 Y. Isaka, Y. Kondo, Y. Kawase, Y. Kuwahara, K. Mori and H. Yamashita, *Chem. Commun.*, 2018, **54**, 9270-9273.
- 46 Y. Horiuchi, T. Toyao, M. Saito, K. Mochizuki, M. Iwata, H. Higashimura, M. Anpo and M. Matsuoka, *J. Phys. Chem. C*, 2012, **116**, 20848-20853.

Table of contents

(graphic maximum size 8 cm x 4 cm and one sentence of text, maximum 20 words, highlighting the novelty of the work)



A hydrophobic Ti doped Zr-based MOF was synthesized and used for photocatalytic H_2O_2 production in two-phase system (aqueous/benzyl alcohol).